

Exploring plasmons weakly coupling to perovskite excitons with tunable emission by energy transfer

Guo-Dong Yan(严国栋), Zhen-Hua Zhang(张振华), Heng Guo(郭衡), Jin-Ping Chen(陈金平),Qing-Song Jiang(蒋青松), Qian-Nan Cui(崔乾楠), Zeng-Liang Shi(石增良), and Chun-Xiang Xu(徐春祥)

Citation: Chin. Phys. B, 2023, 32 (**6**): 067302. DOI: 10.1088/1674-1056/ac921b
Journal homepage: http://cpb.iphy.ac.cn; http://iopscience.iop.org/cpb

What follows is a list of articles you may be interested in

First-principles study of plasmons in doped graphene nanostructures

Xiao-Qin Shu(舒晓琴), Xin-Lu Cheng(程新路), Tong Liu(刘彤), and Hong Zhang(张红)
Chin. Phys. B, 2021, 30 (**9**): 097301. DOI: 10.1088/1674-1056/abe92d

Collective excitations and quantum size effects on the surfaces of Pb(111) films: An experimental study

Yade Wang(王亚德), Zijian Lin(林子荐), Siwei Xue(薛思玮), Jiade Li(李佳德), Yi Li(李毅), Xuetao Zhu(朱学涛), and Jiandong Guo(郭建东)
Chin. Phys. B, 2021, 30 (**7**): 077308. DOI: 10.1088/1674-1056/abfbcd

Enhanced circular dichroism of TDBC in a metallic hole array structure

Tiantian He(何田田), Qihui Ye(叶起惠), Gang Song(宋钢)
Chin. Phys. B, 2020, 29 (**9**): 097306. DOI: 10.1088/1674-1056/aba9ce

Quantization of electromagnetic modes and angular momentum on plasmonic nanowires

Guodong Zhu(朱国栋), Yangzhe Guo(郭杨喆), Bin Dong(董斌), Yurui Fang(方蔚瑞)
Chin. Phys. B, 2020, 29 (**8**): 087301. DOI: 10.1088/1674-1056/ab9698

Selective excitation of multipolar surface plasmon in a graphene-coated dielectric particle by Laguerre Gaussian beam

Yang Yang(杨阳), Guanghua Zhang(张光华), Xiaoyu Dai(戴小玉)
Chin. Phys. B, 2020, 29 (**5**): 057302. DOI: 10.1088/1674-1056/ab7e97

Exploring plasmons weakly coupling to perovskite excitons with tunable emission by energy transfer

Guo-Dong Yan(严国栋)[1], Zhen-Hua Zhang(张振华)[1], Heng Guo(郭衡)[1], Jin-Ping Chen(陈金平)[1], Qing-Song Jiang(蒋青松)[2], Qian-Nan Cui(崔乾楠)[1], Zeng-Liang Shi(石增良)[1], and Chun-Xiang Xu(徐春祥)[1,†]

[1] *State Key Laboratory of Bioelectronics, School of Physics, Southeast University, Nanjing* 210096, *China*
[2] *Faculty of Electronic Information Engineering, Huaiyin Institute of Technology, Huaian* 223001, *China*

(Received 11 July 2022; revised manuscript received 15 August 2022; accepted manuscript online 15 September 2022)

Localized surface plasmon resonance (LSPR) has caused extensive concern and achieved widespread applications in optoelectronics. However, the weak coupling of plasmons and excitons in a nanometal/semiconductor system remains to be investigated via energy transfer. Herein, bandgap tunable perovskite films were synthesized to adjust the emission peaks, for further coupling with stable localized surface plasmons from gold nanoparticles. The degree of mismatch, using steady-state and transient photoluminescence (PL), was investigated systematically in two different cases of gold nanoparticles that were in direct contacting and insulated. The results demonstrated the process of tuning emission coupled to LSPR via wavelength-dependent photoluminescence intensity in the samples with an insulating spacer. In the direct contact case, the decreased radiative decay rate involves rapid plasmon resonance energy transfer to the perovskite semiconductor and non-radiative energy transfer to metal nanoparticles in the near-field range.

Keywords: plasmons, photoluminescence, tunable emission, perovskite

PACS: 73.20.Mf, 78.55.–m, 79.60.–i **DOI:** 10.1088/1674-1056/ac921b

1. Introduction

Localized surface plasmon resonance (LSPR), generally produced by photoexcitation of noble metal nanoparticles, has attracted great attention due to its characteristics of ultra-confined light.[1–4] It has a wide applications in optoelectronics such as SPASERs,[5–7] enhancing light-emitting diodes,[8] all-optical switches,[9] super light absorbers[10] and energy conversion.[11,12] Numerous experiments on the enhancement of light fields and emission have been extensively demonstrated in recent years,[13–18] and there have been many investigations into how surface plasmon resonance enhances the light emission[19–25] between plasmonic nanostructures and emitters. Particularly, the energy transfer process remains to be investigated systematically with regard to the enhancement of the electromagnetic field and emission intensity in the perovskite semiconductor around localized surface plasmonic nanostructures.

There have been many advances in surface plasmon-enhanced light emission, and several types of energy transfer processes have been investigated and explored in different fluorescent systems. Breshike *et al.*[26] developed a nanometal surface energy transfer model that predicted gold nanoparticle (Au NP) size-dependent photoluminescence (PL) quenching of a dye at a fixed separation distance by the modified size-dependent dielectric constant of the gold nanoparticle. Cheng *et al.*[27] optimized an insulating spacer in a monolayer transition metal dichalcogenide–plasmonic system. A one nanometer-thick spacer on silver film had the best PL enhancement at the same temperature. Furthermore, they observed quenching of the temperature-variable PL in the absence of a spacer, but gave no detailed explanation for their observations. Li *et al.*[28] reported localized surface plasmon-enhanced light emission intensity as a function of insulating spacer thickness in core-shell nanostructures. They pointed out that plasmon-induced resonance energy transfer (PIRET) is a non-radiative coherent energy transfer between metal NPs and the semiconductor in the core-shell nanostructures through dipole–dipole coupling, which differs from the unidirectional Förster resonance energy transfer (FRET) process. Another type of non-radiative energy transfer is the direct exchange of electrons between two molecules, involving the overlap of electron clouds or the contact of molecules.[29] This process, called Dexter energy transfer (DET), is different from FRET and is suitable for long-range energy transfer with an intermolecular distance of 5 nm to 10 nm.[30] It is only suitable for short-range energy transfer with intermolecular distances within 1.5 nm. However, investigations on localized surface plasmon–exciton coupling in nanometal/semiconductor systems are limited, and study of the energy process is still ambiguous.

This study aims to achieve a nanometal/perovskite coupling system. For this, perovskite semiconductor films with different emission peaks, realized by the modulation of perovskite composition and small-sized gold nanoparticles, have been prepared. After constructing the system, steady-state PL spectroscopy and micro-region absorption spectroscopy are used to detect the changes in absorbance and emission inten-

[†]Corresponding author. E-mail: xcxseu@seu.edu.cn

© 2023 Chinese Physical Society and IOP Publishing Ltd

sity, and to analyze the enhancement or quenching of photoluminescence under different degrees of detuning between the perovskite films and the LSPR peak. In addition, a two nanometer-thick alumina spacer was introduced into this system to illustrate the fact that the PIRET enhances perovskite PL with higher efficiency than non-radiative energy transfer, and the perovskite exciton emission peak matched the LSPR peak. Time-resolved photoluminescence (TRPL) explicitly demonstrates that radiative decay rates decrease, consistent with the results of steady-state PL spectroscopy. This also partially revealed that the plasmon-induced resonance energy transfer process decreased the excited state decay time, and the non-radiative energy transfer process extended the excited state decay time. This work provides some references for the experimental design of semiconductor device performance that is enhanced by localized surface plasmons. Our study of the resonant coupling of the nanometal/perovskite system could inspire further studies on the energy transfer mechanism of localized surface plasmon–exciton interaction.

2. Results and discussion

2.1. Preparation of gold nanoparticles and perovskites

Gold nanoparticles supporting localized surface plasmons were synthesized using a chemical solution method. A transmission electron microscope (TEM) image of the gold nanoparticles is illustrated in Fig. 1(a). The uniformly dispersed gold nanoparticles, with an average size of about 4 nm, can be clearly seen in Fig. 1(b). According to the particle-size distribution diagram, most of the gold nanoparticles are in the range of 3.5 nm–4.5 nm in size. Precisely, as presented in the inset of Fig. 1(c), the gold nanoparticles were dispersed in n-hexane as a solvent.

Furthermore, in the extinction process of metal nanoparticles, part of the light is absorbed by localized surface plasmon resonance (LSPR), another part is absorbed by exciting the forbidden transition, and the last part is scattered to the far field. Since the particle diameter completely varies in the range of 3.5 nm–4.5 nm in our samples, the scattered part of the extinction cross section may be neglected and the extinction curve corresponds to an absorption curve. Thus, the absorption curve of the smaller metal NPs is attributed to both the forbidden transition and LSPR. In general, the single LSPR peak is described as a Lorentzian curve according to the free electron Drude model, and the forbidden transition is also called interband transition of metal NPs that is electronic transition from the d-band to the conduction band.[31] The absorbance spectrum in Fig. 1(c) appears distinctly as a single resonance about 520 nm, corresponding to LSPR. Therefore, the absorbance spectrum of Au NPs can be divided into localized surface plasmonic absorption of free electron collective oscillation (purple segment curve) and interband transition absorption of bound electrons (red segment curve) by exciting at short wavelengths below 500 nm.[32]

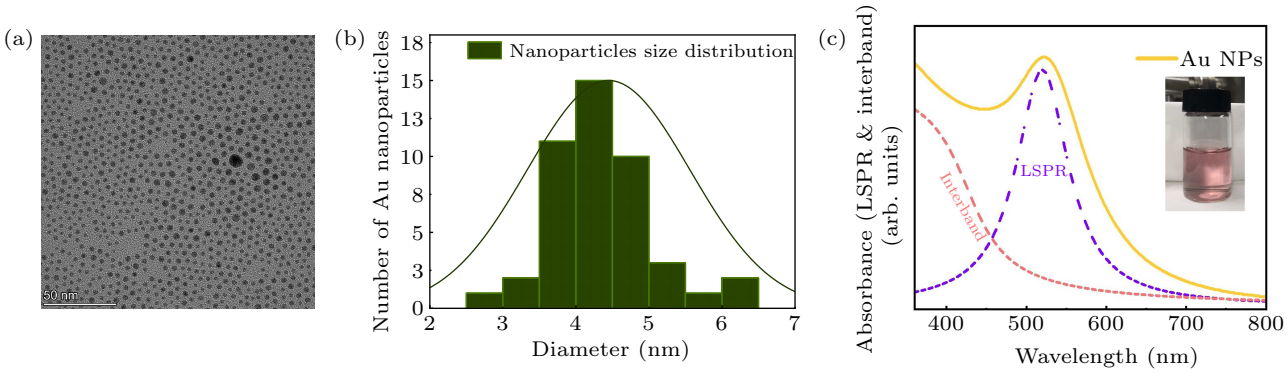


Fig. 1. (a) TEM images, and (b) the size distribution obtained by TEM of Au nanoparticles. (c) Absorbance spectra of Au nanoparticles (inset: an image of Au NPs in glass bottles) divided into absorption curves of the LSPR and the interband transition.

To tune the emission wavelength to match the LSPR peak, we designed four perovskite films of luminescent material on glass sheets (1.5 cm × 1.5 cm) and varied the fluorescence peak position from 470 nm to 536 nm. Scanning electron microscope (SEM) images of the $MAPbBr_{3-x}Cl_x$ films are illustrated in Figs. 2(a)–2(d). All the images show dense and uniform stacked granular film morphology. Using an energy dispersive spectrometer, we acquired the chloride ion content of the $MAPbBr_{3-x}Cl_x$ films as $x = 0$, $x = 0.3$, $x = 0.8$, and $x = 0.9$, corresponding to Figs. 2(a)–2(d), respectively.

In addition, the crystallinity and cubic crystal structure of the initial $MAPbBr_3$ film were verified using x-ray diffraction (XRD) analysis. The XRD pattern of the initial film has the main diffraction peaks in Fig. 2(e) at 15.02°, 21.26°, 30.2°, and 43.2°, corresponding to the (100), (110), (200), and (220) crystal planes of perovskite $MAPbBr_3$,[33,34] respectively. The cubic crystal structure of the perovskite $MAPbBr_{3-x}Cl_x$ is verified using *ex situ* XRD measurements. The peak for a (100) diffraction plane shifts from 15.02° (pure Br), 15.22°, 15.36°, to 15.44°,[35–38] indicating that the chloride ion had exchanged a certain percentage in the $x = 0$, 0.3, 0.8 and 0.9 bromine ion based on the pure $MAPbBr_3$ film in Fig. 2(f). From the ba-

sic morphology, structure and crystallinity, it can be seen that we have successfully synthesized perovskite films with different compositions, namely, different bromine and chloride ion ratios.

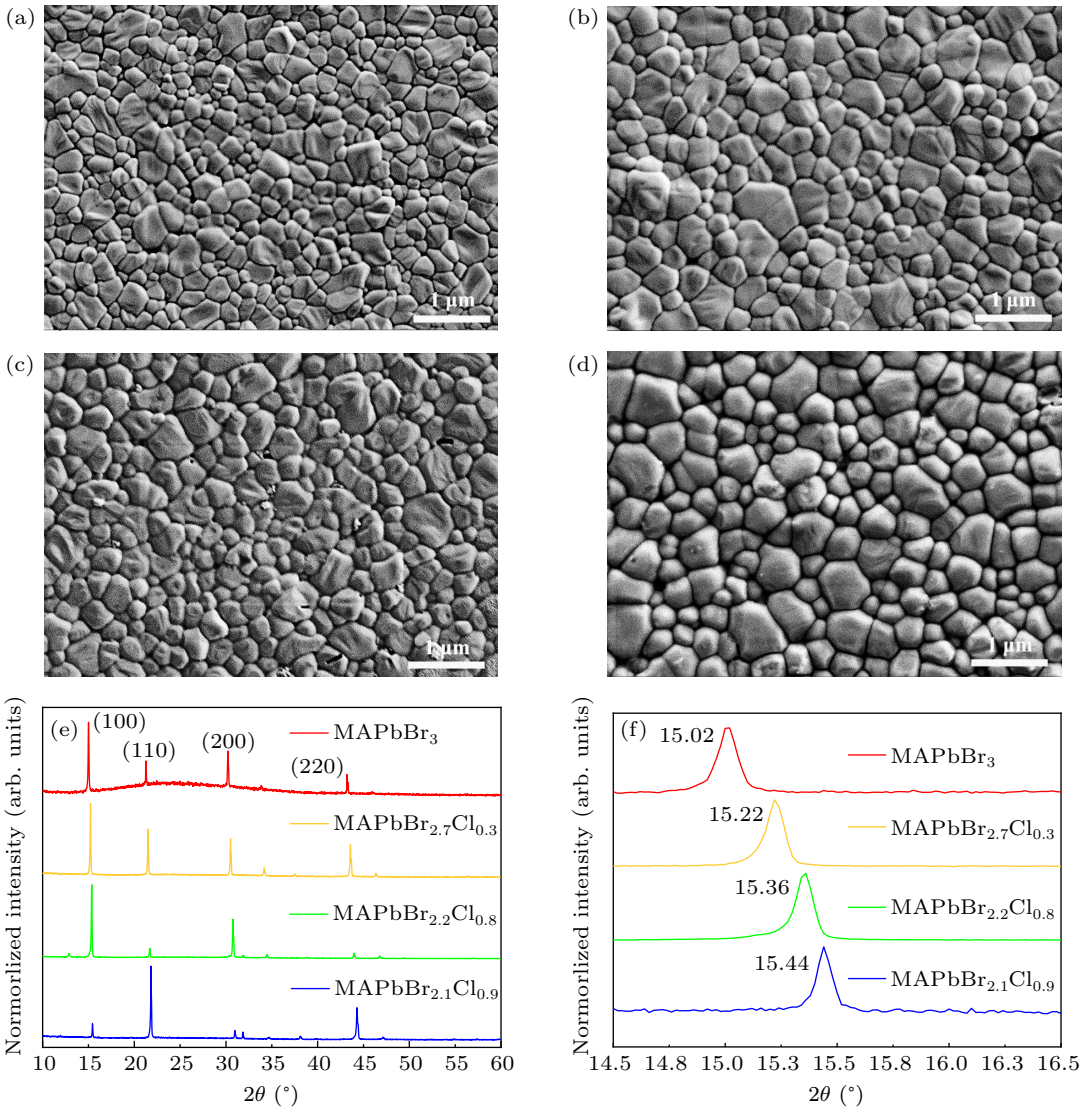


Fig. 2. SEM images of perovskite $MAPbBr_{3-x}Cl_x$ films with successively increased chloride ion content from (a), (b), (c) to (d). (e) Normalized XRD patterns of perovskite $MAPbBr_{3-x}Cl_x$ films. (f) Normalized peaks of (100) diffraction planes from different films.

2.2. Steady-state spectral analysis

Next, the test of the PL and absorbance spectrum of the $MAPbBr_{3-x}Cl_x$ films was performed. Based on changes in the composition of the films, the gradient absorption band edges and PL peaks can be obtained using a steady-state PL spectrometer and micro-zone absorption spectrometer. The normalized absorbance peak grades from 456 nm to 523 nm, corresponding to the normalized PL peak grading from 470 nm to 536 nm, as shown Figs. 3(a) and 3(b). Additionally, we found the emission wavelength of the perovskite $MAPbBr_{2.7}Cl_{0.3}$ at 518 nm in Fig. 3(b) is very close to the LSPR wavelength. This means it may have tuned the emission peak of the perovskite to successfully match the LSPR peak.

Thereafter, the four perovskite films could be combined with the Au NPs in the spacer and in direct contact, respectively. A simple coupling system was used to directly drip the same dose of gold nanoparticle solution onto the four perovskite films, respectively. The fluorescence intensity of the simple coupling system was weakened to varying degrees under a continuous wave laser at 405 nm wavelength. Here, the degree of enhancement or quenching can be described by an enhancement factor (EF), which is equal to the ratio of the film's fluorescence peak area after dripping Au NPs onto the previous counterparts. All EFs less than one have been displayed intuitively by a translucent purple line, as shown in Fig. 3(b). Therefore, Au NPs quenched the fluorescence of the perovskite films to varying degrees in cases of direct contact. In the system with Au NPs in contact with perovskite, fluorescence quenching may result from the fact that the coating of the Au NPs absorbs part of the excitation and emission light and weakens the fluorescence intensity of the perovskite films. In addition, the perovskite film of the emission peak

at the highest overlap with the LSPR peak obtains the largest EF, which can be seen more clearly from the scatter plot in Fig. 4(e). This may result from the fact that the resonant coupling between excitons of the perovskite $MAPbBr_{2.7}Cl_{0.3}$ and localized surface plasmons of excited Au NPs enables the entire system to obtain the largest EF.

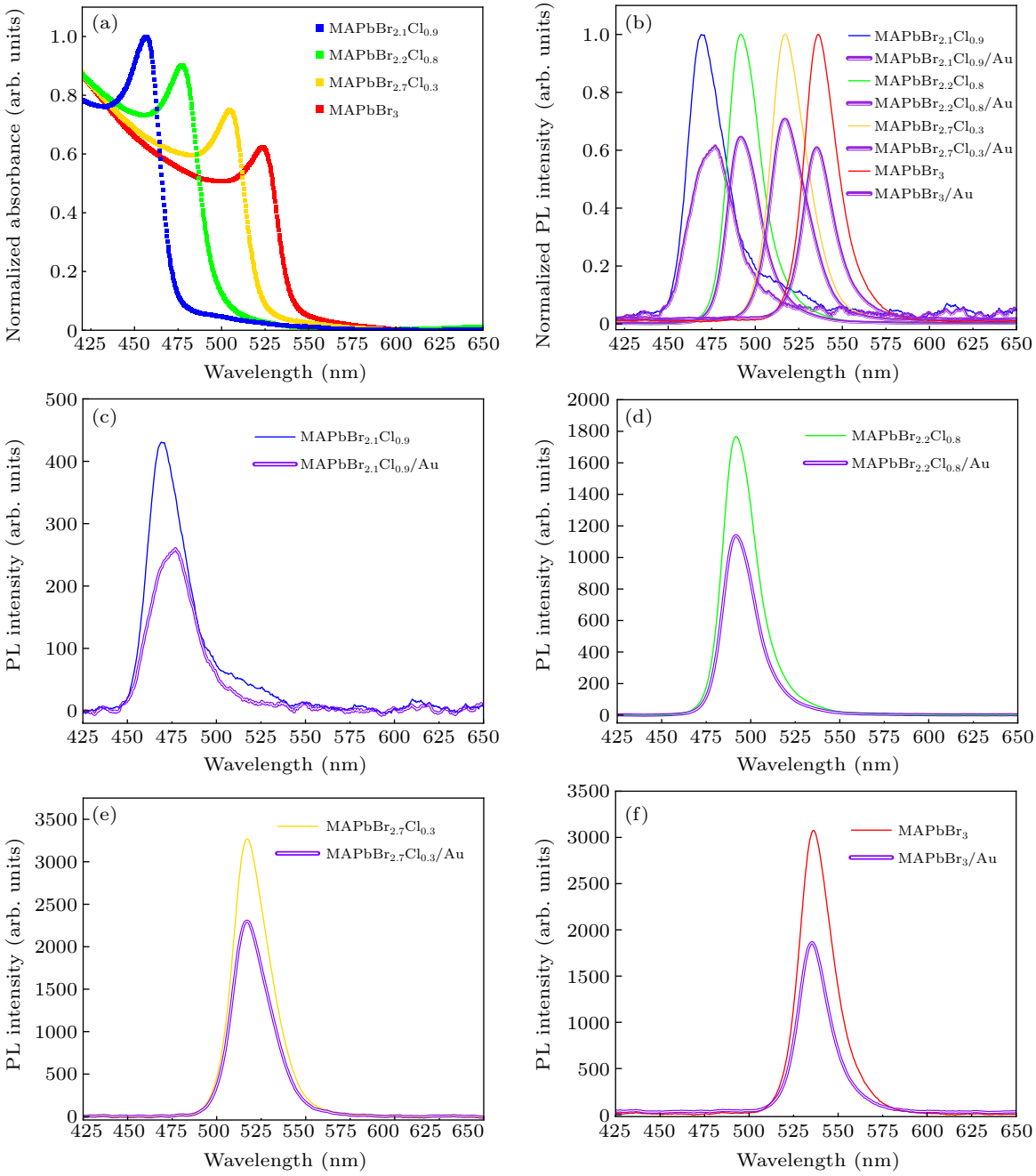


Fig. 3. (a) Normalized absorbance spectra of $MAPbBr_{3-x}Cl_x$ films. (b) Normalized photoluminescence spectra of the perovskite $MAPbBr_{3-x}Cl_x$ films and the relative change in their photoluminescence intensity after dripping Au NPs. (c)–(f) The change in photoluminescence intensity on the single sample decorated by Au NPs.

With regard to the best-known perspective, a widely applied FRET process was proposed to reveal the fluorescence quenching of fluorescent molecules.[26] The energy released from an excited donor could simultaneously excite the ground-state acceptor based on the Coulombic interaction between these two chemical groups. The Dexter energy transfer (DET) is thought to be energy transfer as a result of exchanging electrons at an electron cloud overlap.[29] It (also called Dexter electron exchange) is a fluorescence quenching mechanism in which an excited electron is transferred from one molecule (a donor) to a second molecule (an acceptor) via a non-radiative path. This process requires a wavefunction overlap between the donor and acceptor, which means it can only occur at short distances, typically within 1 nm. These energy transfer mechanisms can be called a non-radiative energy transfer (NET) mechanism. Another energy transfer process, called plasmon-induced resonance energy transfer (PIRET), can harvest visible to near-infrared light energy.[28] In our

nanometal/perovskite system, according to NET, Au NPs will possibly get more energy from the perovskite films at the worse alignment of their PL peaks and the absorption peak of gold nanoparticles in direct contact cases. However, in PIRET, localized surface plasmons will provide the most energy for the perovskite film, with the emission peak matched to the LSPR peak.

To eliminate energy loss by exchanging electrons in a nanometal/perovskite system, an about 2 nm thick Al_2O_3 spacer was deposited on the four perovskite films using pulsed laser deposition, and subsequently dripped the gold nanoparticles onto the perovskite films with the insulating spacer. As a result, the fluorescence intensity of the perovskite films shows different degrees of enhancement under the same continuous wave laser in Figs. 4(a)–4(d), which means that all the EFs are greater than one. The largest enhancement factor can be obtained, as shown in Fig. 4(c), and this means that the perovskite $MAPbBr_{2.7}Cl_{0.3}$ got the most energy compared to the other films in the case of the insulating spacer. The enhancement factors varying with wavelength are displayed intuitively in Fig. 4(f). By comparing Figs. 4(e) and 4(f), we find that the coating of Au NPs to block light is not the main reason for weakening of the fluorescence intensity of perovskite films after depositing the alumina spacer. Moreover, it is found that

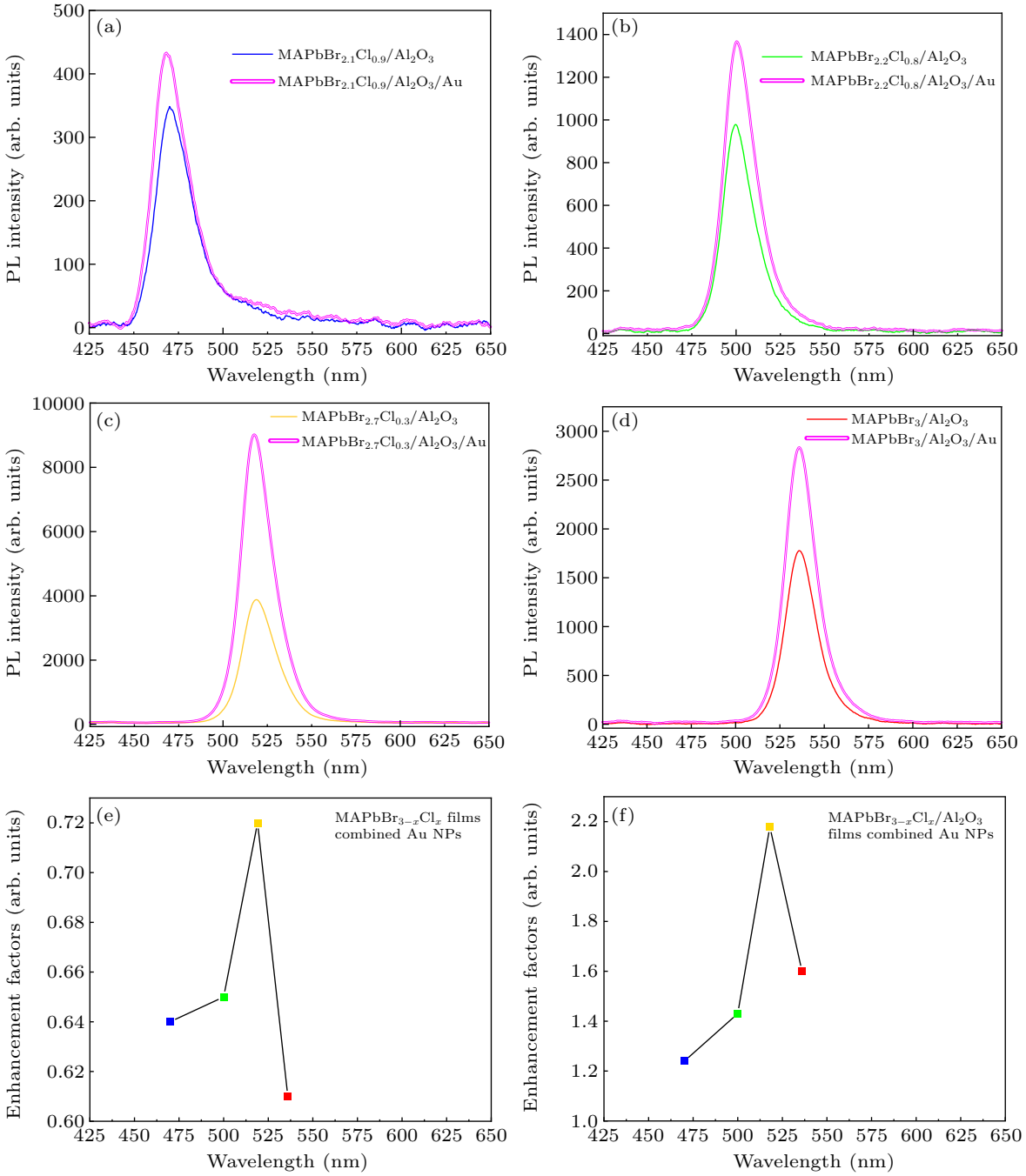


Fig. 4. (a)–(d) The variations of fluorescence intensity for the perovskite films with the alumina spacer after dropping Au NPs. The enhancement factors versus wavelength (e) before depositing alumina and (f) after depositing alumina.

the EFs, as shown in Fig. 4(f), first increase and then decrease as the Cl doping concentration increases. The reason for this is that, depending on the LSPR peak, the semiconductor with the PL peak center closer to its peak center gets bigger enhancement. The PL peak center of the perovskite films in this paper is blue-shifted from 536 nm to 470 nm as the Cl doping concentration increases, while the LSPR peak center is about 520 nm; therefore, the PL intensity of Au/Al_2O_3/perovskite will first increase and then decrease. Furthermore, efficient localized surface plasmon–exciton coupling has occurred due to the largest EF. As mentioned previously, it is evident that different oscillation intensities at different positions of the localized surface plasmonic peak mean different enhancement effects, and the largest enhancement effect is located at the center frequency. In the Au/Al_2O_3/perovskite system, the PIRET can be described as coherent transfer of plasmonic energy to perovskite excitons, which makes the overall emission intensity higher. The FRET can be described as non-radiative energy transfer to the metal NPs, especially when the emission peak matches the absorption peak of Au NPs, as shown in Fig. 4(e).

2.3. Transient photoluminescence measurements

To further explore the carrier behavior of the perovskite semiconductor coupling with localized surface plasmons, time-resolved photoluminescence spectroscopy was performed to uncover the photogenerated carrier behavior of perovskite induced by a possible energy transfer process in the near-resonant coupling system. The fluorescence lifetimes of the perovskite films, with or without Au NPs, were detected using a streak camera under the same power 400 nm pulsed laser (150 fs, 1000 Hz). Isolated perovskite films generally have only one spontaneous emission recombination channel, which is the spontaneous transition of electrons in the excited state. Meanwhile, the decoration of gold nanoparticles will cause an additional spontaneous emission recombination channel, which is the spontaneous transition of electrons in different states after exchanging electrons. Therefore, a single exponential decay function was used to fit the fluorescence lifetime decay curve of isolated perovskite $MAPbBr_{2.7}Cl_{0.3}$, and a biexponential decay function was used to fit the fluorescence lifetime decay curve of the Au/$MAPbBr_{2.7}Cl_{0.3}$ system. The multi-exponential decay function is expressed by

$$I(t) = I_0 + \sum_{i=1}^{n} A_i \exp(-t/\tau_i), \quad \tau_{\text{avg}} = \frac{\sum_{i=1}^{n} A_i \tau_i^2}{\sum_{i=1}^{n} A_i \tau_i}.$$

Here, I_0 is the fit constant, while A_i and τ_i are the amplitude and decay time constant of the i-th component function, respectively. In Fig. 5(a), τ_1 and τ_2 are short and long fluorescence lifetimes, respectively. The τ_{avg} is the average value of the fluorescence lifetimes in multi-exponential decay. According to the results of the fitting decay curve, fluorescence lifetime values have been calculated as exactly shown in Fig. 5(a). The τ_1 is described as a shortened fluorescence lifetime induced by PIRET, and τ_2 is described as extended fluorescence lifetime, mainly induced by DET. The 0.42 ns fluorescence lifetime of the isolated film is extended to the average fluorescence lifetime 0.97 ns, which means that the radiation decay rate Γ_r, corresponding to emission intensity, is reduced. This result is consistent with the weakened emission intensity measured via steady-state PL spectroscopy in Fig. 3(b).

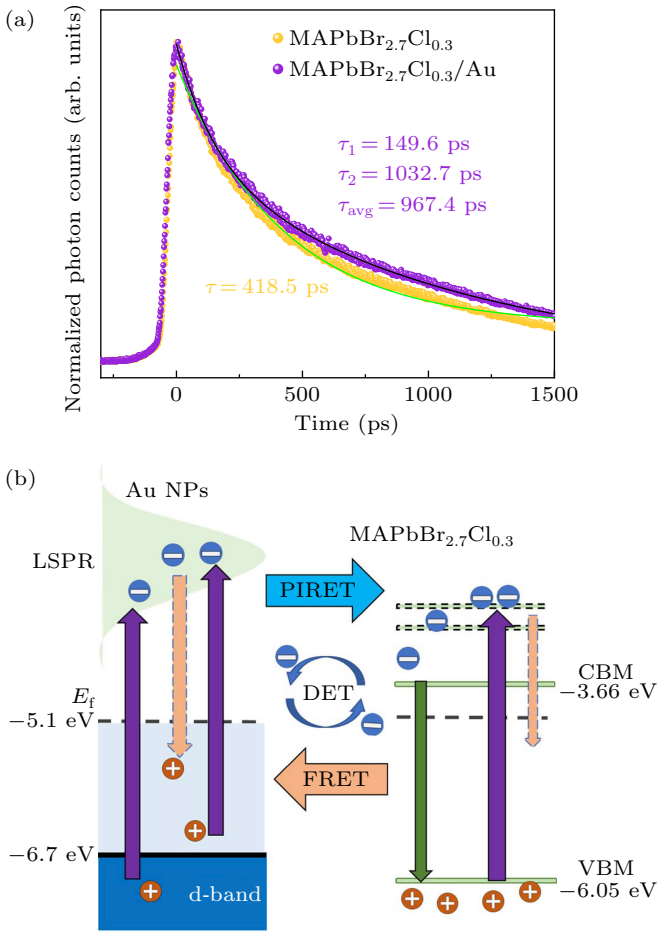


Fig. 5. (a) Normalized time-resolved photoluminescence spectra for the perovskite $MAPbBr_{2.7}Cl_{0.3}$ before and after dripping Au NPs, as well as the fitting fluorescence lifetimes. (b) A schematic diagram of the physical process in the composite system of $MAPbBr_{2.7}Cl_{0.3}$/Au. Purple arrow: photoexcited electronic transition; orange dotted arrow: nonradiative process; green arrow: radiative process; blue bidirectional curved arrow: electron exchange process.

According to the electronic properties of gold nanoparticles with diameters less than 10 nm[39] and semiconductors, a photophysical schematic diagram of the gold nanoparticles and perovskite is given in Fig. 5(b). Photoexcited electronic transition of the perovskite and LSPR, as well as d-band electronic transition of Au NPs occurs, as shown by the purple arrow, when a 400 nm pulsed laser enters the coupling system. The localized surface plasmonic energy is coherently transferred to the semiconductor by FIRET. Thus, oscillating elec-

trons quickly relax to hot electrons and the electrons in the conduction band of the semiconductor also relax, as shown by the orange dotted arrow, which results in a short lifetime of 0.15 ns. Then, the overlapping of the electron wave-functions of gold nanoparticles and perovskite films is likely to cause electron exchange between them; therefore, the DET process occurs in the gold–semiconductor direct contact case. Thus, the energy of the excited electrons in the semiconductor is lost. Moreover, the photons radiated by the semiconductor will be partially reabsorbed by FRET due to the matching of the emission peak and the gold absorption peak. The electronic exchange process of DET may quench semiconductor fluorescence and result in a long lifetime of 1.03 ns in Fig. 5. Hence, the average fluorescence lifetime is longer than the fluorescence lifetime of isolated perovskite semiconductors. Finally, the recombination channel caused by PIRET and NET leads to the total reduced radiative decay rate, and then the fluorescence lifetime is extended.

3. Conclusion

In summary, the optical properties of multiple emission wavelengths are achieved via multiple perovskite $MAPbBr_{3-x}Cl_x$. The single LSPR peak is derived from the absorption spectrum of the synthesized small-sized Au NPs. From the configuration of the Au/perovskite system, the different degrees of coupling between excitons and localized surface plasmons are observed by the steady-state PL spectrum; the emission intensities of the original isolated films are weakened to different degrees. Based on the existing research results, the possible energy transfer, including FIRET for energy into perovskite and NET undergoing energy dissipation, have been discussed and categorized. After the introduction of the alumina spacer, the emission intensity of the perovskite films has been enhanced to different degrees, indicating that the DET effect is eliminated, and the perovskite $MAPbBr_{2.7}Cl_{0.3}$ still obtains the biggest EF. Moreover, the process of tuning emission coupled to LSPR has been demonstrated by wavelength-dependent EFs. Furthermore, the measurement of lifetimes via TRPL spectroscopy also illustrates energy transfer processes in the Au/$MAPbBr_{2.7}Cl_{0.3}$ system. NET can weaken perovskite fluorescence more, which results in a long lifetime of 1.03 ns. Therefore, the average fluorescence lifetime, 0.97 ns, of the whole system is longer than the 0.42 ns lifetime of isolated perovskites. This work could promote the effective utilization of localized surface plasmon effects and may inspire further research on localized surface plasmon-mediated studies on the energy transfer mechanism of localized surface plasmons on metals interacting with semiconductor excitons.

Appendix A: Methods

Materials PbI_2, N,N-dimethylformamide (DMF) and hydrochloric acid (HCl) were purchased from Sigma-Aldrich. Methylamine hydrochloride (MACl) and methylammonium bromide (MABr) were purchased from Xi'an Polymer Light Technology Cory Company. Oleylamine was purchased from Shanghai D-chem. N-octane was purchased from Shanghai Macklin Biochemical Technology Co., Ltd.

Gold chloride trihydrate and borane-tert-butylamine complex powder were purchased from Aladdin, and n-hexane was purchased from Nanjing Chemical Reagent Co., Ltd. The absolute ethanol was from Sinopharm Chemical Reagent Co., Ltd.

Preparation of $MAPbBr_{3-x}Cl_x$ films Initially, the raw PbI_2 material (purity 99.99%) was placed in a vacuum deposition chamber, and the ion-cleaned glass sheet (1.5 cm × 1.5 cm) was kept upside down over the material. Then, it was preheated at 200 °C for about 15 min in a nitrogen atmosphere, and the air was pumped three times to remove the entrained moisture therefrom. Next, the temperature of the vacuum chamber was increased to 300 °C at a rate of 50 °C/min, then increased to 360 °C at a rate of 10 °C/min, and finally increased to 370 °C at a rate of 1 °C/min, followed by reaction for 12 h. By lowering the temperature of the glass substrate to room temperature in the same manner as before, the final film thus obtained was annealed in a high-temperature tube furnace at 10 °C/min to a central temperature of 180 °C for 1–2 h and returned to room temperature.

Quartz boats containing 300 mg MAI powder and PbI_2 film were placed in the middle and downstream of the tube furnace, respectively, at 10 °C per minute to increase the central temperature to 110 °C for 4 h, and finally the $MAPbBr_3$ film precursor was obtained.[38] Next, the quartz boats, with 100 mg of MACl powders and $MAPbBr_3$ film precursor, were placed in the middle and downstream of the tubular furnace, respectively. Then, the tubular furnace was pumped down to 20 Pa and 30 sccm nitrogen was introduced. Then, it was heated up to 80 °C at 10 °C/min and maintained the reaction temperature for around 30 min, 90 min and 130 min, thus obtaining different $MAPbBr_{3-x}Cl_x$ films.

Preparation of Au nanoparticles A mixture of 10 mL oleylamine and 10 mL n-octane was added to a 50 mL double-necked round-bottom flask, and stirred for 5–10 min under a constant temperature water bath at 20 °C. Then, 0.1 g solid chloroauric acid was added to the round-bottomed flask, and stirred for 5–10 min under a nitrogen protective atmosphere. Another 0.25 g tert-butylammonium borane powder was dissolved in 1 mL oleylamine mixture, and then poured into the round-bottomed flask, and stirring was stopped after about 1 h. Finally, the original reaction solution was settled in 60 mL absolute ethanol to concentrate the solution by centrifugation,

and the bottom precipitate was dispersed in 10 mL n-hexane to obtain approximately a few nanometers of gold nanoparticles.

Characterizations A field emission scanning electron microscope (Carl Zeiss Ultra Plus) and x-ray energy dispersive spectrometer (EDS, Oxford X-Max 50) were used to obtain the morphology and elemental compositions of the perovskite film, respectively. The XRD pattern of the sample was obtained using x-ray diffraction analysis (Cu $K\alpha$, Rigaku Corporation). The pulsed laser deposition (PLD) system is mainly composed of a laser and vacuum deposition system. The laser is a KrF excimer laser (Coherent Company, the United States) with 248 nm wavelength, a frequency range of 1–50 Hz and a maximum energy of 700 mJ. The vacuum deposition system was purchased from Shenyang Scientific Instrument Co., Ltd., Chinese Academy of Sciences, and the model is a PLD-300a. It adopts a two-stage vacuum system consisting of a mechanical pump and a molecular pump, and the ultimate vacuum is 6.67×10^{-5} Pa. The PL decay lifetimes of samples were measured using an optically triggered streak camera system (Optronic GmbH SC-10).

Acknowledgments

Project supported by the National Key R&D Program of China (Grant Nos. 2017YFA0700503 and 2018YFA0209101) and the National Natural Science Foundation of China (Grant Nos. 61821002, 11734005, 62075041, and 61704024).

References

[1] Hutter E and Fendler J H 2004 *Adv. Mater.* **16** 1685
[2] Agrawal A, Cho S H, Zandi O, Ghosh S, Johns R W and Milliron D J 2018 *Chem. Rev.* **118** 3121
[3] Mu X, Hu L, Cheng Y, Fang Y and Sun M 2021 *Nanoscale* **13** 581
[4] Zhu X P, Zhang S, Shi H M, Chen Z Q, Quan J, Xue S W, Zhang J and Duan H G 2019 *Acta Phys. Sin.* **68** 247301 (in Chinese)
[5] Noginov M A, Zhu G, Belgrave A M, Bakker R, Shalaev V M, Narimanov E E, Stout S, Herz E, Suteewong T and Wiesner U 2009 *Nature* **460** 1110
[6] Meng X, Kildishev A V, Fujita K, Tanaka K and Shalaev V M 2013 *Nano Lett.* **13** 4106
[7] Galanzha E I, Weingold R, Nedosekin D A, Sarimollaoglu M, Nolan J, Harrington W, Kuchyanov A S, Parkhomenko R G, Watanabe F, Nima Z, Biris A S, Plekhanov A I, Stockman M I and Zharov V P 2017 *Nat. Commun.* **8** 15528
[8] Chen S H, Yu C F, Wang C J, Chen S H, Chen Y D, Chen T C and Lin C F 2016 *Org. Electr.* **38** 337
[9] Ono M, Hata M, Tsunekawa M, Nozaki K, Sumikura S, Chiba H and Notomi M 2020 *Nat. Photonics* **14** 37
[10] Yu P, Besteiro L V, Wu J, Huang Y, Wang Y, Govorov A O and Wang Z 2018 *Opt. Express* **26** 20471
[11] Kong X T, Khorashad L K, Wang Z and Govorov A O 2018 *Nano Lett.* **18** 2001
[12] Yu P, Besteiro L V, Huang Y, Wu J, Fu L, Tan H H, Jagadish C, Wiederrecht G P, Govorov A O and Wang Z 2019 *Adv. Opt. Mater.* **7** 1800995
[13] Marin B C, Hsu S W, Chen L, Lo A, Zwissler D W, Liu Z and Tao A R 2016 *ACS Photonics* **3** 526
[14] Meng F, Hu J H, Wang H, Zou G Y, Cui J G and Zhao Y 2019 *Acta Phys. Sin.* **68** 237801 (in Chinese)
[15] Ren Q H, Zhang Y, Lu H L, Chen H Y, Zhang Y, Li D H, Liu W J, Ding S J, Jiang A Q and Zhang D W 2016 *Nanotechnology* **27** 165705
[16] Rashed A R, Habib M, Das N, Ozbay E and Caglayan H 2020 *New J. Phys.* **22** 093033
[17] Bayles A, Carretero-Palacios S, Calió L, Lozano G, Calvo M E and Míguez H 2020 *J. Mater. Chem. C* **8** 916
[18] Zhu Y Z, Chen J P, Cui Q N, Guo H, Li Z X, Shi Z L and Xu C X 2021 *Nano Research* **14** 4288
[19] Russell K J, Liu T L, Cui S and Hu E L 2012 *Nat. Photonics* **6** 459
[20] Matsuda K, Ito Y and Kanemitsu Y 2008 *Appl. Phys. Lett.* **92** 211911
[21] Chen R A and Sun X 2015 *Chin. Phys. Lett.* **32** 083601
[22] Viste P, Plain J, Jaffiol R, Vial A, Adam P M and Royer P 2010 *ACS Nano* **4** 759
[23] Sen T and Patra A 2012 *J. Phys. Chem. C* **116** 17307
[24] Abadeer N S, Brennan M R, Wilson W L and Murphy C J 2014 *ACS Nano* **8** 8392
[25] Zhu Y Z, Cui Q N, Chen J P, Chen F, Shi Z L, Zhao X W and Xu C X 2021 *ACS Appl. Mater. Interfaces* **13** 6820
[26] Breshike C J, Riskowski R A and Strouse G F 2013 *J. Phys. Chem. C* **117** 23942
[27] Cheng F, Johnson A D, Tsai Y, Su P H, Hu S, Ekerdt J G and Shih C K 2017 *ACS Photonics* **4** 1421
[28] Li J, Cushing S K, Meng F, Senty T R, Bristow A D and Wu N 2015 *Nat. Photonics* **9** 601
[29] Wang Z J, Zhao J, Zhou Z, Qi Y G and Yu J S 2017 *Chin. Phys. B* **26** 047302
[30] Lai R C, Liu Y Y, Luo X, Chen L, Han Y Y, Lv M, Liang G J, Chen J Q, Zhang C F, Di D W, Scholes G D, Castellano F N and Wu K F 2021 *Nat. Commun.* **12** 1532
[31] Sönnichsen C, Franzl T, Wilk T, Plessen G V, Feldmann J, Wilson O and Mulvaney P 2002 *Phys. Rev. Lett.* **88** 077402
[32] Scholl J A, Koh A L and Dionne J 2012 *Nature* **483** 421
[33] Liu Y, Zhang Y, Zhao K, Yang Z, Feng J, Zhang X, Wang K, Meng L, Ye H, Liu M and Liu S 2018 *Adv. Mater.* **30** 1707314
[34] Jiang B, Chen S L, Cui X L, Hu Z T, Li Y, Zhang X Z, Wu K J, Wang W Z, Jiang Z M, Hong F, Ma Z Q, Zhao L, Xu F, Xu R and Zhan Y Q 2019 *Acta Phys. Sin.* **68** 246801 (in Chinese)
[35] Lu H, Zhang H, Yuan S, Wang J, Zhan Y and Zheng L 2017 *Phys. Chem. Chem. Phys.* **19** 4516
[36] Yang J X, Zhang P, Wang J P and Wei S H 2020 *Chin. Phys. B* **29** 108401
[37] Liu Y, Yang Z, Cui D, Ren X, Sun J, Liu X, Zhang J, Wei Q, Fan H, F Yu, Zhang X, Zhao C and Liu S 2015 *Adv. Mater.* **27** 5176
[38] Zhang Z H, Wei H, Manohari A G, You D T, Wang R, Li Z X, Liu W, Chen J P, Zhu Y Z, Shi Z L, Cui Q N, Li S and Xu C X 2021 *Adv. Opt. Mater.* **9** 2002186
[39] Visikovskiy A, Matsumoto H, Mitsuhara K, Nakada T, Akita T and Kido Y 2011 *Phy. Rev. B* **83** 165428